ACADEMIA MATERIALS SCIENCE

Research Article
Published: 2024-04-30
https://doi.org/10.20935/AcadMatSci6206

Enhancing the interlaminar adhesion of carbon fiber composites via carbon nanotube sheets

Ning Bian[1], Yao Ren[1], Ashutosh Shrivastava[2], Zhong Wang[3], Duck J. Yang[2], Samit Roy[4], Ray Baughman[3], Hongbing Lu[1,*]

Academic Editor: Raul D.S.G. Campilho

Abstract

Spread tow carbon fiber composites are receiving increased attention for diverse applications in space and sports gear due to their thin form, which is suitable for deployable structures, and high tensile strength. Their compressive strength, however, is much lower than their tensile strength due to low interlaminar strength. Herein we report a facile technique to enhance their performance through interlaminar insertion of aligned carbon nanotube (CNT) sheets. The inserted CNT sheets also provide electrical conductivity in the composites even at a low CNT loading below the electrical percolation threshold established for CNT-filled composites. Mechanical and electrical characterization was conducted on the CNT sheet-inserted composites and the baseline composites. Results show that the CNT sheets increase the compressive strength by 14.7% compared with the baseline. Such an increase is attributed to the increased adhesion provided by the inserted CNT sheets at the interface between neighboring plies, which also increases the interlaminar shear strength by 33.0% and the interfacial mode-II fracture toughness by 34.6% compared with the baseline composites without inserting CNT sheets. The well-aligned CNT sheet structure maintained between the neighboring plies contributed to a 64.7% increase in electrical conductivity compared with the baseline composites. The findings indicate that the insertion of well-aligned ultrathin CNT sheets in the interlaminar region of a spread tow carbon fiber composite provides significant enhancement in mechanical and electrical performance, paving the path toward applications where both mechanical and electrical performances are crucial, such as for structural health monitoring, lightning protection, and de-icing in aircraft and wind blades.

Keywords: *spread tow carbon fiber, compressive strength, interlaminar shear strength (ILSS), mode-II fracture toughness, fractographic analysis*

Citation: Bian N, Ren Y, Shrivastava A, Wang Z, Yang DJ, Roy S, Baughman R, Lu H. Enhancing the interlaminar adhesion of carbon fiber composites via carbon nanotube sheets. *Academia Materials Science* 2024;1. https://doi.org/10.20935/AcadMatSci6206

1. Introduction

Carbon fiber-reinforced polymers (CFRPs) are finding increasing applications across various sectors such as aerospace (including rockets, aircraft, and air taxis), energy (wind turbine blades, hydrogen storage tanks, etc.), automotive (particularly in electric vehicles), civil engineering (including pedestrian bridges, CFRP rebars, and traffic poles), naval applications (such as unmanned stealth ships), and sports equipment (such as tennis rackets and bicycles) [1–7]. The increased applications of CFRPs are due to their exceptional attributes including lightweight, high-specific strength and stiffness, and low thermal expansion [1, 3, 6].

Among CFRPs, spread tow carbon fiber composites have recently gained significant attention due to their unique properties, including lighter weight and straighter fibers, which enhance the mechanical performance [8, 9]. However, like many CFRPs, they face challenges in compressive and shear strength, primarily due to weak interlaminar shear strength (ILSS) and low interfacial shear strength (IFSS) at the fiber/matrix interface [10–14]. To address this, reinforcing the interlaminar region is vital for improving load transfer efficiency between the plies in the laminate, consequently enhancing the overall mechanical properties of CFRPs.

Numerous approaches have been reported to enhance the interlaminar regions of CFRPs. Among these approaches, carbon nanotubes (CNTs) are often used due to their extraordinary physical, chemical, and mechanical properties including a very large specific surface area (up to 1,300 m^2/g), high modulus (up to 1 TPa), and high strength (up to 150 GPa) [15–17]. The prevalent approach reported in the literature is to disperse CNTs in the polymer matrix, which is used to impregnate carbon fibers to make composites improve the matrix dominant properties such as flexural strength/modulus and ILSS of composites. This process usually starts with mechanically mixing CNTs with a

[1]Department of Mechanical Engineering, The University of Texas at Dallas, Richardson, TX, 75080, USA.
[2]Department of Chemistry and Biochemistry, The University of Texas at Dallas, Richardson, TX, 75080, USA.
[3]Alan G. MacDiarmid NanoTech Institute, The University of Texas at Dallas, Richardson, TX, 75080, USA.
[4]Department of Aerospace Engineering and Mechanics, University of Alabama, Tuscaloosa, AL, 35487, USA.
*email: hongbing.lu@utdallas.edu

polymer matrix, and then using the resin to prepare composites to take advantage of the extraordinary properties of CNTs in CFRPs. A large body of work [18–23] has demonstrated interlaminar strength improvement by adding CNTs to the matrix of composites. However, this approach usually leads to agglomeration of CNTs, which prevents their uniform dispersion from manufacturing high-quality composites. For instance, Sanchez et al. [22] introduced CNTs to the matrix of a carbon fiber composite with different CNT loadings by calendaring using a three-roller mill and characterized the mechanical properties of composites. Their results showed that with 0.1 wt% CNTs doping in the epoxy matrix, the ILSS increased by 5.6%, and a slight increase was observed in tensile and flexural strength. A slightly higher dosage of CNTs (such as 0.3 wt%) did not yield performance improvement in the composites anymore. Similarly, Santos et al. [24] also mixed CNTs into the matrix of a CFRP, and they reported that a higher dosage (0.089 wt%) of CNTs does not benefit the improvement of mode-I fracture toughness of CFRPs compared with a lower dosage (0.043 wt%) of CNTs mixed with CFRP.

CNT grafted on carbon fibers is another way to improve the interfacial and interlaminar properties of CFRPs [25–32]. Grafting CNT on a carbon fiber is a chemical process in vapor deposition. This process is usually conducted at elevated temperatures and involves catalyst coating and formation, which tends to degrade the axial properties of the carbon fibers. Numerous groups [33–37] have observed that both the tensile strength and modulus of carbon fiber reduced after the chemical vapor deposition (CVD) process. For example, Zhang et al. [35] reported a 75% reduction in the tensile strength of carbon fiber after the CVD process. In addition, high CNT grafting density hinders the polymer matrix from flowing onto the carbon fiber surfaces, which resulted in weak interface bonding strength [29], and the uniformity of CNT growth on carbon fibers was not always satisfactory.

To overcome the limitations of the traditional approaches in enhancing CFRP properties, recent research has turned to the use of carbon nanotube (CNT) sheets. Liu et al. [38] and Mu et al. [39] have demonstrated the potential of incorporating CNT sheets in polymer fiber composites, such as CFRPs, to improve the mechanical and electrical performance. However, a challenge arises due to the inherent thinness of CNT sheets pulled from CNT forests. When integrated into continuous fiber composites, these sheets impact only a very thin interphase region between adjacent plies, as indicated in references [40] and [41], leading to limited performance enhancement.

Interestingly, CFRPs constructed with thinner ply thickness have shown increased strength and a reduction in transverse cracks compared to those with thicker plies [7, 42]. This suggests a promising direction for further improvement: using even thinner plies in CFRPs. Such an approach would allow the CNT sheets to penetrate a larger volume fraction of the composite material. Consequently, this could not only provide further mechanical enhancements but also potentially improve the electrical properties of the composites. This approach represents a significant step toward fully leveraging the benefits of CNT sheets in advanced composite materials like CFRPs.

While carbon fibers are highly electrically conductive, their polymer matrix composites are in general not electrically conductive. As such, in applications where lightning protection and de-icing are needed, additional metal network is needed. To reduce the weight of the metal network, numerous researchers have made attempts to enhance the electrical conductivity. The electrical conductivity of CFRPs is highly anisotropic and depends on the orientation of carbon fibers. In the carbon fiber direction, CFRPs are electrically conductive because of the inherent conductivity of carbon fibers but they are insulated in both transverse and thickness directions due to the intrinsic electrical insulation of the polymer matrix. To resolve this issue, CNTs, with high electrical conductivity, are often introduced. When CNTs having a good dispersion reach a percolation threshold or higher, the composites exhibit electrical conductivity [43–45].

To address the above-mentioned issues, we herein report the insertion of ultrathin well-aligned CNT sheets into the neighboring plies of thin spread tow carbon fiber fabric to make composites. The aerogel CNT sheets pulled from CNT forests were inserted into the interlaminar region between adjacent plies of CFRPs, followed by ethanol sorption and desorption to form CNT xerogel for enhanced mechanical properties. In spread tow carbon fiber fabrics, spread tow tapes are aligned in both warp and weft directions. Such spread tow fiber plies are much thinner than a typical carbon fiber tow fabric so that more CNT sheets can be inserted between adjacent plies to provide additional enhancement. Moreover, spread tow fabric does not usually contain crimps, which reduce the risk of the formation of possible pin holes and resin shrinkage area [46, 47]. The reduced pin holes and shrinkage will further lead to a strong adhesion with the inserted CNT sheets and matrix, leading to increased interlaminar performance. This increased adhesion is also anticipated to increase the fracture toughness when a crack is along the interface between two neighboring plies. Due to the well-aligned structure in CNT sheets, electrical conductivity can be achieved even when the CNT loading is below the percolation threshold reported in the literature, which will be examined in this work.

We made CFRP composites by inserting ultrathin well-aligned CNT sheets at the interface between neighboring plies of the spread tow carbon fiber fabrics. We measured the compressive strength, IFSS, and fracture toughness of the CNT sheet-inserted composites. The mechanisms for the enhancement of fracture toughness were examined by fractographic analysis. The electrical conductivity of CNT sheet-inserted composites was also measured. This paper is organized as follows: the materials used and characterization method are described in Section 2, the results are presented and discussed in Section 3, and conclusions are drawn in Section 4.

2. Materials and characterization methods

In this section, CNT sheets are drawn from the CNT forest grown on a silicon wafer and are subsequently inserted into the interlaminar region of CFRPs. We describe the preparation and insertion of CNT sheets into the CFRPs to prepare composite specimens. We also describe the characterization methods for mechanical properties and electrical conductivity.

2.1. CNT sheet-inserted spread tow carbon fiber fabrics

The TeXtreme 12k UTS 50 spread tow carbon fiber fabrics were used to make composites. The spread tow fabric has 80 grams per

square meter (gsm) in the warp direction and 40 gsm in the weft direction, and the fabric was constructed with a 20-mm width tape in a woven pattern. The matrix material was Epon 862 epoxy resin from Westlake Epoxy, and the hardener was Epikure curing agent W. Ultrahigh purified multi-walled CNT sheets were drawn from 300-µm tall, vertical-aligned CNT forest grown on a 6-inch silicon substrate provided by Lintec NSTC. The sheet has an aerial density of approximately 0.025 gsm, and the CNTs have an outer diameter of approximately 10 nm [48].

2.2. Fabrication of the CNT-spread tow carbon fiber composites

Multi-walled CNT sheets were drawn from the CNT forest (**Figure 1a**), which were then coupled with spread tow carbon fiber fabrics along the warp direction of the fabrics. Both the spread tow carbon fiber fabrics and CNT sheets were bonded together by sorption and desorption of ethanol, which consolidated the as-drawn CNT aerogel sheets to CNT xerogel sheets. Subsequently, CNT-spread tow carbon fiber fabrics were dried at ambient temperature overnight, and the dried CNT-spread tow carbon fiber fabric is shown in **Figure 1b**. Thus, the CNT sheets were maintained in the well-aligned structure during fabrication. The surface morphology of CNT-spread tow carbon fiber fabrics was observed under a scanning electron microscope (SEM) as shown in **Figure 1c** and **1d**. The SEM image in **Figure 1c** showed that CNT sheets were successfully wrapped around carbon fiber filaments. The SEM image in **Figure 1d** showed the as-received carbon fiber without CNT. Only approximately 60% of spread tow carbon fiber fabrics were covered with CNT sheets (**Figure 1b**) so that the baseline spread tow CFRPs were made on the remaining uncovered 40% under identical processing conditions with the CNT-spread tow CFRPs. The dried CNT-spread tow carbon fiber fabrics were then stacked together (**Figure 1e**) to fabricate testing coupons (**Figure 1f**) via vacuum-assisted resin infusion molding (VARIM). The curing temperature was set to 75°C, and the curing time was set to 20 hours following a two-hour post-cure at 120°C.

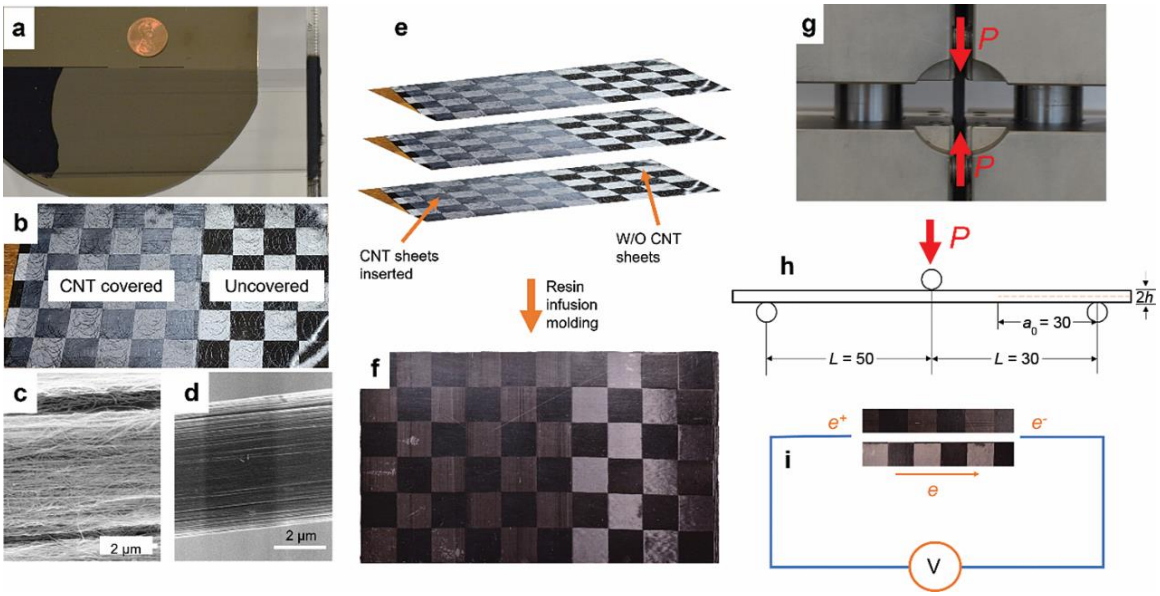

Figure 1 • The fabrication flow and testing of CNT-spread tow CFRPs. (a) A CNT sheet was drawn from a vertical-aligned CNT forest. (b) Dry CNT-spread tow carbon fiber fabric after ethanol desorption. The CNT sheets were aligned with the warp direction of spread tow carbon fiber fabric, and approximately 60% of the fabric area was covered with CNT sheets. (c) An SEM image of the CNT sheet inserted in carbon fiber; it shows that the CNT sheet was successfully wrapped around carbon fiber along the fiber direction. (d) An SEM image of as-received carbon fiber without CNT sheet insertion. (e) Stacking sequence of CNT-spread tow carbon fiber fabrics. (f) CNT-spread tow carbon fiber composite testing coupon made by resin infusion molding. (g) Compression test configuration: the red arrows represent loading directions. (h) Mode-II fracture toughness test configuration: the red arrow indicates the loading direction. (i) Electrical conductivity test configuration: the orange arrow indicates the current flow direction across the composite specimen.

Twenty-three plies of spread tow carbon fiber-CNT fabrics were laid up through the stacking sequence in **Figure 1e** to make a 3.2-mm thick plate for the combined loading compression (CLC) test and the short beam shear (SBS) test (for testing interlaminate shear strength). A total of 32 spread tow carbon fiber fabric layers were stacked together in the same sequence to make CFRP plates for the mode-II fracture toughness. Both the 16th and 17th plies were coupled with a monolayer of ultrathin CNT sheet; these two CNT-CF plies were consolidated and dried before stacking together. A 13-µm thick fluorinated ethylene propylene (FEP) film was inserted with care between the 16th ply and 17th ply as a delamination initiator. The fabricated testing coupons were then cut into testing specimens for testing as shown in **Figure 1g–i**.

2.3. Mechanical characterization

The compressive strength along the fiber warp direction (80 gsm) was determined by the CLC test following ASTM D6641 [49], and the dimensions of each specimen were 140 × 13 × 3.2 mm. The compression test was conducted under the displacement-controlled condition at 1.3 mm/min. Four specimens were tested for each composite. The fractured surface of a failed specimen was observed under a Leica DMi8 inverted optical microscope to investigate the failure mode of the specimen.

The ILSS of the CNT-spread tow carbon fiber composite was determined using the SBS test following ASTM D2344 [50]. Short-beam specimens were cut along the warp direction, and the nominal dimensions of each specimen are 30 × 10 × 3.2 mm. The

actual dimensions of each specimen were measured and used in the calculation of ILSS. The span-to-depth ratio was set to 6:1 instead of 4:1 to prevent local crushing/buckling to maintain a large zone of uniform shear stress [14]. The central loading was provided by a 10-mm pin to prevent any indentation into the surface of the beam specimen. The diameter of the two support pins was 3 mm. The displacement rate applied by the loading nose in the center of the beam specimen was 1 mm/min in all the SBS tests. Four specimens were tested for each composite.

Mode-II fracture toughness test was conducted following ASTM D7905 [51]. The end-notched fracture (ENF) specimens were cut by waterjet out of both the baseline plate and 0.025 wt% CNT sheet-inserted plate, respectively. The specimens have a nominal dimension of 210 × 20 × 4.46 mm, with a delamination initiator of 70 mm. The side of the specimen facing the camera was sprayed with a thin layer of speckles for visual determination of the crack. The specimens were marked with vertical lines at 20, 30, and 40 mm from the tip of the insert before the mode-II fracture test. The schematic diagram of the ENF specimen is shown in **Figure 2a**, and the test configuration is shown in **Figure 2b**. An Instron 5900 series testing apparatus (Instron, Norwood, MA, USA) was used as the testing platform. The load was applied to the specimen by a 3-point bending fixture, and the loading pin and the support pins have a diameter of 10 mm. The loading pin was placed 20, 30, and 40 mm from the tip of the insert, respectively, while the span was 100 mm. A deflectometer was used to measure the actual displacement at the center of the specimen, and a camera was used to record the crack initiation and propagation. The specimen compliance was calibrated using the method described in ASTM D7905, and the displacement rate was 0.5 mm/min.

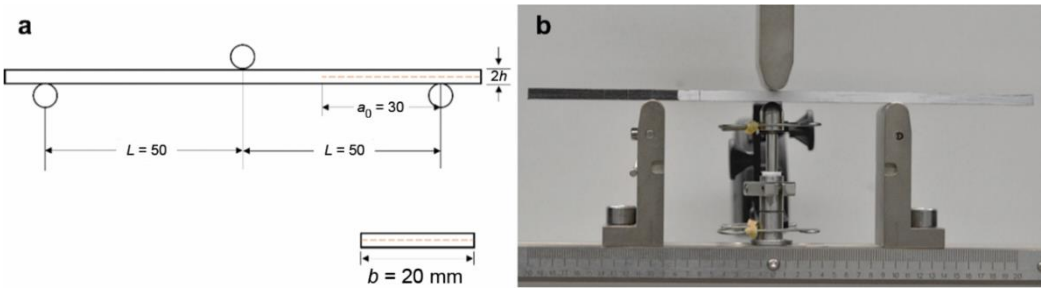

Figure 2 • End-notched fracture (ENF) specimen of baseline CFRP and CNT-spread tow CFRP. (a) The schematic diagram shows the nominal dimensions of the ENF specimen used in this work. The orange dashed line represents the inserted FEP film. (b) An ENF specimen was mounted on the testing apparatus. The sides of all specimens facing the camera were coated with a thin layer of speckle for the determination of crack propagation. The mid-span displacement was measured by a deflectometer.

A total of three specimens were tested for each composite. The mode-II interlaminar fracture toughness was calculated via the compliance calibration method (CCM) using the equation:

$$G_{\mathrm{IIc}} = \frac{3mP_{\max}^2 a_0^2}{2B},$$

where G_{IIc} is the mode-II interlaminar fracture toughness, m is the compliance calibration coefficient, $P_{\max}$ is the maximum force in the load-deflection curve, a_0 is the initial crack length, and B is the specimen width.

2.4. Fractography analysis and electrical conductivity measurement

For examination of the morphology of the specimen after mode-II delamination, a Zeiss SIGMA 500 VP scanning electron microscope (Zeiss, Oberkochen, Germany) was used to conduct the fractography analysis on failed samples for both composites. The samples were cut from the delamination growth region of the ENF specimens with the same distance from the end for both the baseline composite specimen and 0.025 wt% CNT-spread tow CFRP specimen.

The electrical conductivity was measured using a Keithley 2400 source meter (Tektronix, Beaverton, OR, USA). The resistance of the samples was measured along the fiber warp direction by applying voltages between the probes, and the electrical conductivity of the CNT-spread tow carbon fiber composite along the fiber warp direction is calculated by $S = L/RA$, where S is the electrical conductivity of the sample, L is the length between two probes, R is the resistance, and A is the cross-sectional area of the sample. Three specimens for each composite were used for measuring the electrical conductivity, and ten measurements were made from each specimen.

3. Results and discussion

The carbon fiber volume fractions, compressive strength along the fiber warp direction, the ILSS, and mode-II fracture toughness of the CFRPs with and without inserted CNT sheets were investigated. Results are reported and discussed in this section.

Optical micrographs as shown in **Figure 3** show that the carbon fiber composites with and without insertion of CNT sheets have almost identical carbon fiber volume fractions at approximately 67%, and no difference is seen between the baseline composites (without insertion of CNT sheets) and CNT-spread tow composites, which indicated that the introduction of CNT sheets does not change the structure of CFRPs.

The compressive strength of spread tow carbon fiber composites with different CNT loadings is plotted in **Figure 4**. The compressive strength along the warp direction of spread tow carbon fiber composite improved with the insertion of CNT sheets reinforcement in the interlaminar region; a 0.025 wt% CNT loading in the composite yields an increase in the compressive strength by 14.7%, and the composite with 0.05 wt% CNT loading shows a 6.6% increase in compressive strength. The compressive strength of composites is governed by the shear strength in the interphase region with a thickness of 100 nm or less [40, 41]. The introduction of two layers of CNT sheets increased the asperity and mechanical interlocking of this region, thus directly enhancing the mechanical behavior.

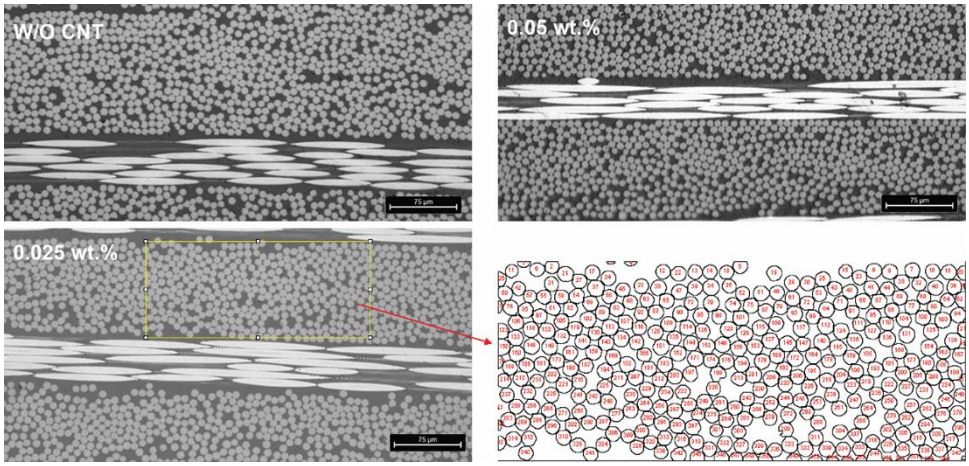

Figure 3 • Optical microscope images on the cross-section of composites with different CNT loadings. The bottom right image shows the selected individual carbon fiber filaments from the cross-section of the composite samples using watershed algorithm.

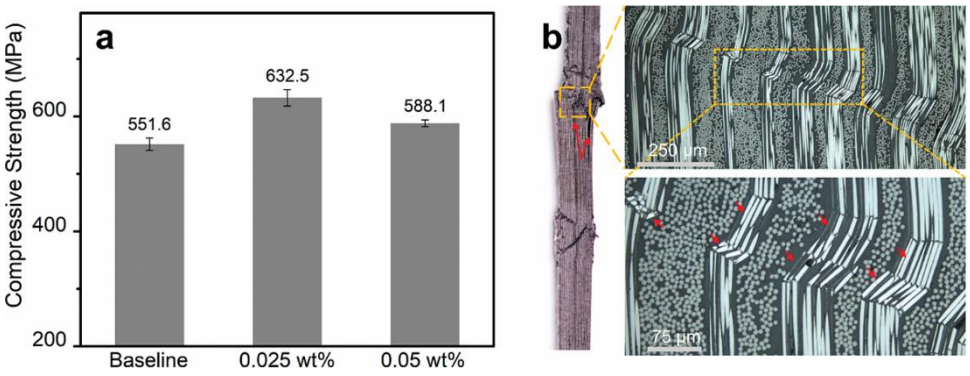

Figure 4 • The compressive properties of CNT-spread tow carbon fiber composites with different CNT loadings. (a) The compressive strength of CNT-spread tow carbon fiber composites. (b) The failure mode of CNT-spread tow carbon fiber composites. The red arrows in the photo of the fractured sample show the delamination failure due to the shift-down of transverse plies, and the red arrows in the microscope image show the kink-band that is induced by microcracking in the load-aligned fiber tows.

The relatively straighter carbon fibers in the spread tow carbon fiber fabrics compared with the regular tow carbon fiber fabrics reduced the possibility of forming wrinkles and folds, resulting in higher compressive strength when compared with the traditional woven carbon fiber composites. The compressive strength of baseline spread tow CFRPs is 551.6 MPa. For the 0.025 wt% CNT-spread tow CFRPs prepared herein, the compressive strength is 632.5 MPa, representing 14.7% enhancement over the baseline composites.

It is noted that the compressive strength of the regular tow woven CFRPs is in the range of 400–500 MPa [52, 53]. However, multi-walled CNT sheets were joined by van der Waals force between neighboring CNTs and neighboring CNT sheets and, as such, exhibited low normal and shear strength [54, 55]; with the increase in the number of CNT layers, the shear load transfer decreases [56]. Therefore, the increase in the number of CNT sheets from two to four leads to a lower compressive strength compared with the case of the insertion of the two CNT sheets into the composite.

The failure mode of the CNT-spread tow carbon fiber composites after the CLC test was observed under an optical microscope. The sample after the CLC test was first embedded in epoxy with care and then polished for optical microscopy, and the micrographs are shown in **Figure 4b**. The two-dimensional woven structure of the CNT-spread tow carbon fiber composite leads to a combined delamination and shear failure mode. The adjacent horizontal carbon fiber tows shift down and separate from the vertical carbon fiber tows upon longitudinal compression, leading to delamination between plies as shown in the arrow-pointed area of the failed specimen in **Figure 4b**, while in the fiber longitudinal direction, the kink-band was observed in the fiber tows, which is induced by microcracking under the applied axial load. However, no difference was observed between the CNT sheet-inserted carbon fiber composite and the baseline composite.

The load-deflection curves of both the baseline and CNT-spread tow carbon fiber composites under the SBS testing are plotted in **Figure 5a**. Laminate mismatches were observed at the edge of the SBS specimens for both composites as shown in the inset image of **Figure 5a**. A nearly linear increase of the curves was observed up to 0.3 mm deflection, then delamination occurred after the curves reached the maximum load. The spread tow composite with CNT sheets inserted between adjacent plies also exhibits a higher stiffness as depicted in the load-deflection curves in **Figure 5a**. This illustrates that the nanocomposite formed by the insertion of CNT sheets in the interlaminar region of spread tow carbon fiber composites provided improved bending stiffness and critical load at the onset of instability to the in-plane shear load during the SBS test. The ILSS of composites with different CNT loading ratios are plotted as a bar chart in **Figure 5b**. Interleaving CNT sheets with spread tow carbon fiber/epoxy composite shows an increase in the ILSS, while a higher concentration of CNTs does not provide additional

improvement of the ILSS anymore. The CNT-spread tow carbon fiber composite with 0.025 wt% CNT has the highest ILSS (48.4 MPa), which is 33.0% higher than that of the baseline composite. The 0.05 wt% CNT-spread tow carbon fiber composite exhibits an increase of ILSS by 22.0% compared with the baseline composite.

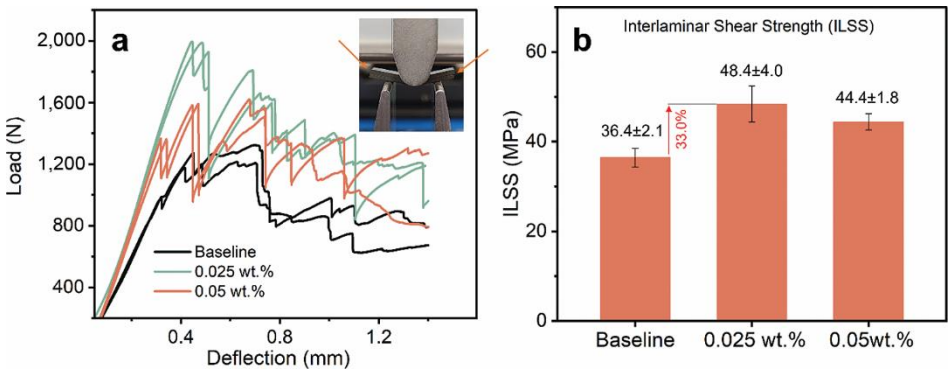

Figure 5 • The interlaminar shear properties of CNT-spread tow carbon fiber composites with different CNT loadings. (a) Representative load-deflection curves of CNT-spread tow carbon fiber composites. The inset image shows the delaminated specimen due to the shear load transfer. (b) The bar chart shows the ILSS and standard deviation of spread tow carbon fiber composites with different CNT loadings.

The electrical conductivity of the CNT-spread tow carbon fiber composite was measured using the two-probe method along the warp direction of the spread tow carbon fiber fabrics. The results are plotted as a bar chart in **Figure 6**. The electrical conductivity improved by introducing CNT sheets to the interlaminar region of spread tow carbon fiber composites. Adding more CNT sheets between plies yields higher electrical conductivity due to the well-aligned structure and high electrical conductivity of CNT sheets, and straighter carbon fibers in spread tow carbon fiber fabric.

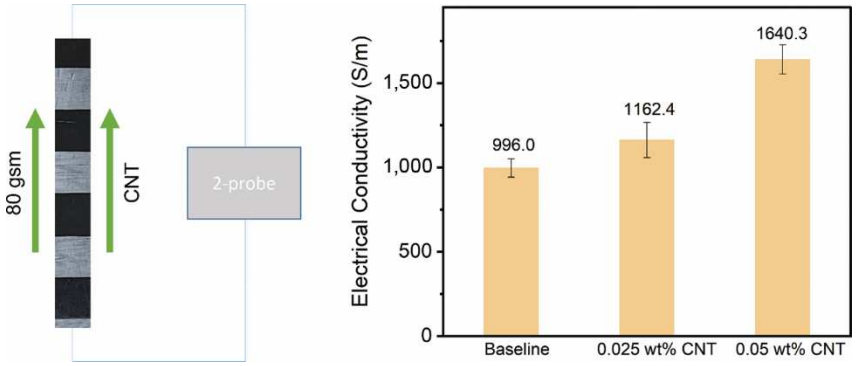

Figure 6 • Electrical conductivity of the CNT-spread tow carbon fiber composites with different CNT loadings. The electrical conductivities were measured along the warp direction of spread tow carbon fiber composites, and 0.05 wt% CNT-spread tow carbon fiber composite exhibits the highest electrical conductivity.

Compared with the baseline spread tow carbon fiber composite, the electrical conductivity increased by 16.7%, from 996.0 S/m to 1,162.4 S/m for 0.025 wt% CNT-spread tow carbon fiber composite. For the 0.05 wt% CNT-spread tow carbon fiber composite, the electrical conductivity increased by 64.7%, from 996.0 S/m to 1,640.3 S/m. The increased electrical conductivity in CNT-spread tow carbon fiber composite demonstrates their potential for applications in structural health monitoring [57, 58], de-icing, and lightning protection in aircraft and wind blades [59, 60].

The above results indicated that the insertion of CNT sheets into the spread tow carbon fiber composites improved their mechanical performance, and a preeminent improvement was demonstrated for spread tow carbon fiber composite with 0.025 wt% CNT loading. As such, the mode-II fracture toughness was compared only between the baseline composite and the composites with 0.025 wt% CNT loading in the following section.

The ENF specimens of the baseline and 0.025 wt% CNT CFRPs were conditioned at 60°C for eight hours before the mode-II delamination test, and then all specimens were tested under room temperature at a humidity of 50% ± 10%. The specimen compliance calibration at the loading point was performed following ASTM D7905 [51], and the specimens were loaded and unloaded within their elastic region at crack lengths of 20 mm and 40 mm, respectively. The fracture test was conducted at a crack length of 30 mm. The compliance C at each crack length then was determined by a linear least squares regression from the displacement and force curves, and the compliance calibration coefficients A and m were calculated using the equation: $C = A + ma^3$. The representative compliance versus crack length cube curves are shown in **Figure 7**; both curves yielded reasonable goodness of fitting, R-square of 0.9996 for baseline CFRP and R-square of 0.9997 for 0.025 wt% CNT CFRP. As illustrated in **Figure 7**, CFRP with 0.025 wt% CNT sheets insertion shows a higher m value than that of baseline CFRP; meanwhile, the A value is lower. The compliance coefficients of both baseline and 0.025 wt% CNT CFRPs are summarized in **Table 1**; the numbers in parentheses show the standard deviations for each coefficient.

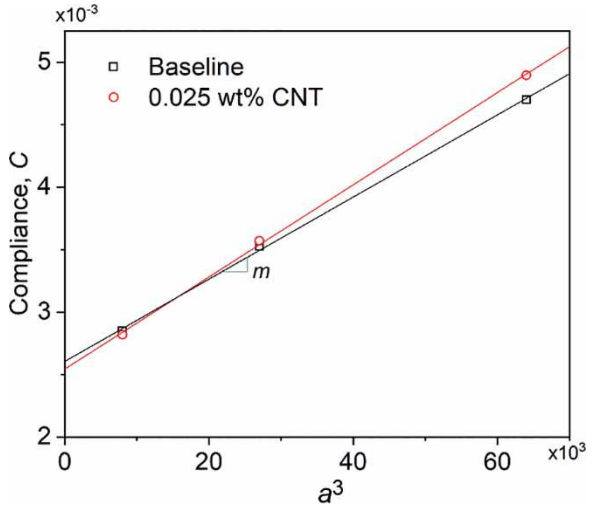

Figure 7 • Representative compliance versus crack length cubed curves of baseline and 0.025 wt% CNT CFRPs. The CFRP containing 0.025 wt% CNT percentage shows a higher *m* value than the baseline CFRP. The compliance is used to determine the crack length.

Table 1 • Compliance coefficients of baseline and 0.025 wt% CNT CFRPs

	A (mm/N)	*m* ($N^{-1}•mm^{-2}$)
Baseline	2.7×10^{-3} (8.2×10^{-5})	3.1×10^{-8} (2.2×10^{-9})
0.025 wt% CNT	2.5×10^{-3} (1.1×10^{-4})	3.9×10^{-8} (2.2×10^{-9})

The representative force versus displacement curves of both composites were plotted as shown in **Figure 8a**; both composites exhibited linear elastic response until the peak forces. There were neither evident crack observations from the video nor apparent force drops before the peak force from the force-displacement curves; therefore, the peak force was identified as the corresponding force at the initiation of the crack under mode-II loading, and the values of peak forces were used to calculate mode-II interlaminar fracture toughness.

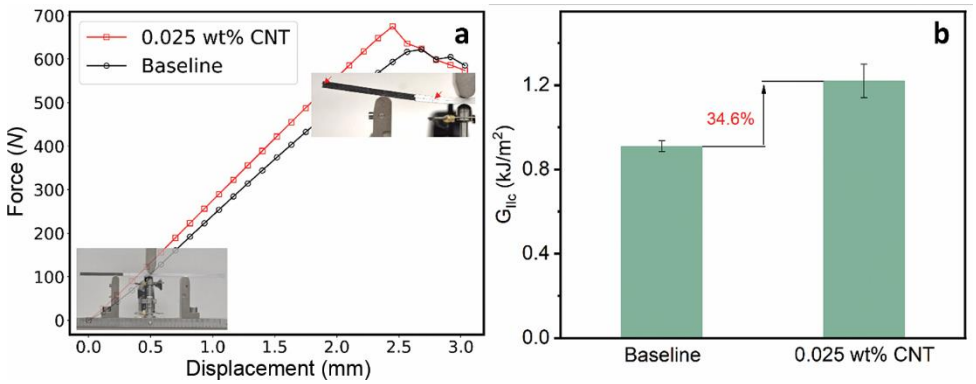

Figure 8 • Mode-II delamination of baseline and 0.025 wt% CNT CFRPs. (a) The representative curve of force versus displacement for both composites. The inset images show the testing configuration of the specimen under loads. A deflectometer was used to measure the mid-span deflection. (b) A bar chart showing the interlaminar fracture toughness of both composites. CFRP with 0.025 wt% CNT sheets insertion in the interlaminar region showed a 34.6% increase in G_{IIc}, which indicated that the inserted CNT sheets are responsible for increased energy absorption for the in-plane shear load.

The values of mode-II interlaminar fracture toughness for both baseline and 0.025 wt% CNT CFRPs are shown in **Figure 8b**. The average G_{IIc} of baseline CFRP was calculated as 908.4 J/m², and the average G_{IIc} of CFRP with 0.025 wt% CNT inserted in the interlaminar region was calculated as 1,222.8 J/m². The interlaminar fracture toughness of CFRP increased by 34.6% due to the increased loading bearing and compliance after the insertion of CNT sheets in the interlaminar region. The increased toughness is attributed to two aspects: (1) CNT increases the Young's modulus of the epoxy matrix due to the formation of CNT/epoxy nanocomposite, which provides a gradual load transfer between plies to reduce stress concentration at the interphase region, and (2) the CNT provides intimate contact between two neighboring plies to increase the adhesion. This finding also agrees with the result obtained by the SBS test, in which case the ILSS was increased by 33% by introducing 0.025 wt% CNT sheets to the interlaminar region.

The fracture mechanism of both baseline and 0.025 wt% CFRPs under mode-II loading was examined with a high-resolution SEM. The failed ENF specimens for both CFRPs were cut in the crack propagated zone for SEM fractography analysis. The representative SEM fractographic images of baseline CFRP were shown in **Figure 9**, and the representative SEM fractographic images of 0.025 wt% CNT CFRP were shown in **Figure 10**. The fracture surface of the baseline composite was relatively clean and smooth, and a typical brittle fracture with hackle markings was observed due to the intensive in-plane shear loading. This shear-induced fracture feature also has been reported by others [61–64]. There was little resin left on the surface of the carbon fiber near the crack initiation zone. This indicated that the baseline composite has poor resistance to the in-plane shear force and resulted in a low mode-II interlaminar fracture toughness.

As for 0.025 wt% CNT CFRP, more resin was left on the surface of the carbon fiber after mode-II loading, and a similar hackle pattern away from the crack propagation direction was observed as shown in **Figure 10a** and **10b**. The resin river pattern was also observed between stitches of carbon fiber filaments as shown in **Figure 10c** and **10d**. The interlaminarly inserted CNT sheets increased the fracture toughness of the interphase region between neighboring plies. Moreover, the well-aligned structure of inserted CNT sheets formed a connected network as shown in **Figure 10c** and **10d** that increases adhesion, and it helps retain resin on the surface of carbon fiber, which also can absorb more

energy during crack initiation and propagation. In addition, the high stiffness of CNT sheets gives rise to relatively lower local strains under in-plane shear loads compared with the baseline without CNT, which helped bridge the in-plane shear-induced matrix cracking as observed in **Figure 10d**. This in turn delayed the propagation of the cracks compared with the baseline CFRP.

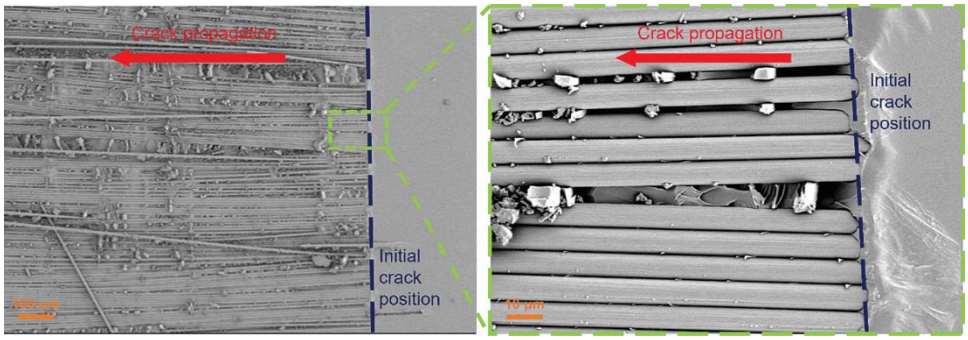

Figure 9 • SEM fractographic images of the fractured zone of the baseline CFRP specimen. The image on the right shows an enlarged view of the fracture surface. It exhibited a clean and smooth carbon fiber surface after mode-II fracture, which indicated poor adhesion between carbon fibers and epoxy matrix.

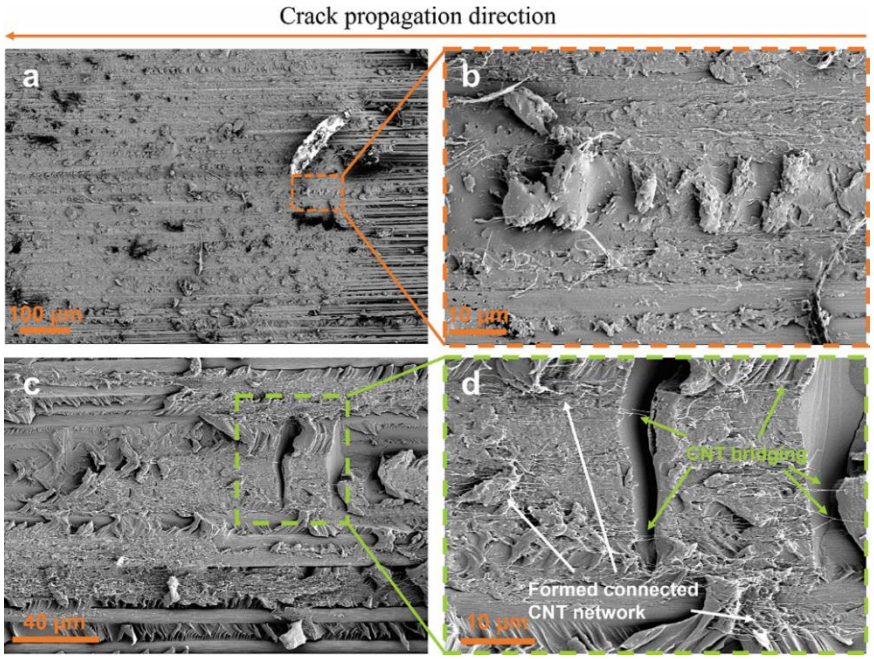

Figure 10 • SEM fractographs showing the fractured zone of the 0.025 wt% CNT CFRP specimen. (a) Surface morphology of 0.025 wt% CNT CFRP after mode-II delamination. (b) Enlarged view of the selected feature showing the river wave feature due to in-plane shear and the formed CNT network to the resin. (c) and (d) The formed CNT network on the fracture surface and CNT bridging the matrix crack.

4. Conclusion

In this work, the well-aligned CNT sheets were inserted into the neighboring plies of spread tow carbon fiber fabrics to make composites via VARIM. The CNT sheets were maintained in a well-aligned structure in the composite. The composite formed with thinner spread tow fabrics and inserted well-aligned CNT sheets demonstrated a 14.7% improvement in compressive strength. The increase in compressive strength is attributed to a 33.0% enhancement in the ILSS and a 34.6% improvement in mode-II fracture toughness. Meanwhile, the maintained, well-aligned structure in CNT sheets in the spread tow composite provides significantly improved electrical conductivity by 64.7% with a low CNT loading even below the electrical percolation threshold for other CNT-filled composites. The results indicate that the insertion of well-aligned CNT sheets directly to the interlaminar region of a spread tow carbon fiber composite improved in the mechanical and electrical performance significantly. The optimal CNT loading was found to be 0.025 wt%, and a further increase in the loading of CNT sheets does not provide continuous enhancement of mechanical properties compared with the lower CNT loading. More research is required to understand the basic mechanism behind this effect.

Acknowledgment

H.L. thanks the support of the Louis A. Beecherl Jr. Chair.

Funding

The research was funded by the National Science Foundation under CMMI-2219347 and CMMI-1636306, Department of Energy under DE-NA0003962 and DE-NA-0003525, Air Force grant FA8650-23-C-5006, Office of Naval Research grant N68335-18-C-0368, Air Force Office of Scientific Research grant

N68335-19C-0303, NSF WindSTAR I/UCRC Center (under NSF grant numbers IIP-1362033 and IIP-1916776), and Robert A. Welch Foundation grant AT-0029.

Author contributions

Conceptualization, N.B. and H.L.; methodology, N.B. and H.L.; formal analysis/testing, N.B. and A.S.; writing—original draft preparation, N.B.; writing—review and editing, N.B., Y.R., A.S., Z.W., D.J.Y., S.R., R.B. and H.L.; supervision, H.L.; funding acquisition, H.L. All authors have read and agreed to the published version of the manuscript.

Conflict of interest

The authors declare no conflict of interest.

Data availability statement

Data supporting these findings are available within the article, at https://doi.org/10.20935/AcadMatSci6206, or upon request.

Institutional review board statement

Not applicable.

Informed consent statement

Not applicable.

Sample availability

Only the tested samples are available upon request.

Additional information

Received: 2024-02-15

Accepted: 2024-04-03

Published: 2024-04-30

Academia Materials Science papers should be cited as *Academia Materials Science 2024*, ISSN 2997–2027, https://doi.org/10.20935/AcadMatSci6206. The journal's official abbreviation is *Acad. Mat. Sci.*

Publisher's note

Copyright

References

1. Deierling PE, Zhupanska OI. Experimental study of high electric current effects in carbon/epoxy composites. Compos Sci Technol. 2011;71(14):1659–64.
2. Feraboli P, Miller M. Damage resistance and tolerance of carbon/epoxy composite coupons subjected to simulated lightning strike. Compos Part A Appl Sci Manuf. 2009; 40(6-7):954–67.
3. Luo R. Friction performance of C/C composites prepared using rapid directional diffused chemical vapor infiltration processes. Carbon. 2002;40(8):1279–85.
4. Griffith DT, Cao D, Lu H, Qian D. Composite materials in wind energy: design, manufacturing, operation, and end-of-life. IOP Conf Ser Mater Sci Eng. 2023;1293(1):012002.
5. Luo H, Lu G, Roy S, Lu H. Characterization of the viscoelastic behavior of bismaleimide resin before and after exposure to high temperatures. Mech Time Depend Mater. 2013;17:369–99.
6. Luo H, Roy S, Lu H. Dynamic compressive behavior of unidirectional IM7/5250-4 laminate after thermal oxidation. Compos Sci Technol. 2012;72(2):159–66.
7. Sihn S, Kim RY, Kawabe K, Tsai SW. Experimental studies of thin-ply laminated composites. Compos Sci Technol. 2007;67(6):996–1008.
8. Borg C. An introduction to spread tow reinforcements: part 1–manufacture and properties. Reinf Plast. 2015;59(4):194–8.
9. El-Dessouky HM, Lawrence CA. Ultra-lightweight carbon fibre/thermoplastic composite material using spread tow technology. Compos Part B Eng. 2013;50:91–7.
10. Kokkada P, Roy S, Lu H. Carbon nanotube sheet scrolled fiber composite for enhanced interfacial mechanical properties. Proceedings of the American Society for Composites: Thirty-First Technical Conference, 2016, Tuscaloosa.
11. Prusty RK, Rathore DK, Ray BC. CNT/polymer interface in polymeric composites and its sensitivity study at different environments. Adv Colloid Interface Sci. 2017;240:77–106.
12. Wang X, et al. Modeling the compressive buckling strain as a function of the nanocomposite interphase thickness in a carbon nanotube sheet wrapped carbon fiber composite. J Appl Mech. 2019;86(10):1.
13. Wang X, et al. The interfacial shear strength of carbon nanotube sheet modified carbon fiber composites. In: Amirkhizi A, Notbohm J, Karanjgaokar N, DelRio FW, editors. Challenges in mechanics of time dependent materials, Vol. 2, Proceedings of the Society for Experimental Mechanics Series. Cham: Springer International Publishing; 2021. p. 25–32
14. Koirala P, et al. Using ultra-thin interlaminar carbon nanotube sheets to enhance the mechanical and electrical properties of carbon fiber reinforced polymer composites. Compos Part B Eng. 2021;216:108842.

15. Peigney A, Laurent C, Flahaut R, Bacsa RR, Rousset A. Specific surface area of carbon nanotubes and bundles of carbon nanotubes. Carbon. 2001;39(4):507–14.

16. Treacy MMJ, Ebbesen TW, Gibson JM. Exceptionally high Young's modulus observed for individual carbon nanotubes. Nature. 1996;381(6584):6584.

17. Demczyk BG, et al. Direct mechanical measurement of the tensile strength and elastic modulus of multiwalled carbon nanotubes. Mater Sci Eng A. 2002;334(1):173–8.

18. Zhao Z, et al. Mechanical, thermal and interfacial performances of carbon fiber reinforced composites flavored by carbon nanotube in matrix/interface. Compos Struct. 2017; 159:761–72.

19. De Greef N, et al. The effect of carbon nanotubes on the damage development in carbon fiber/epoxy composites. Carbon. 2011;49(14):4650–64.

20. Zhou HW, et al. Carbon fiber/carbon nanotube reinforced hierarchical composites: effect of CNT distribution on shearing strength. Compos Part B Eng. 2016;88:201–11.

21. Kim MT, Rhee KY, Lee JH, Hui D, Lau AKT. Property enhancement of a carbon fiber/epoxy composite by using carbon nanotubes. Compos Part B Eng. 2011;42(5,):1257–61.

22. Sánchez M, Campo M, Jiménez-Suárez A, Ureña A. Effect of the carbon nanotube functionalization on flexural properties of multiscale carbon fiber/epoxy composites manufactured by VARIM. Compos Part B Eng. 2013;45(1):1613–9.

23. Srivastava VK, et al. Effect of nanomaterial on mode I and mode II interlaminar fracture toughness of woven carbon fabric reinforced polymer composites. Eng Fract Mech. 2017;180:73–86.

24. Santos RM, et al. Multiscale carbon fibre–reinforced polymer (CFRP) composites containing carbon nanotubes with tailored interfaces. Fatigue Fract Eng Mater Struct. 2019;42(7):1521–33.

25. Lee G, et al. A facile method for preparing CNT-grafted carbon fibers and improved tensile strength of their composites. Compos Part A Appl Sci Manuf. 2015;69:132–8.

26. Peng Q, et al. Chemically and uniformly grafting carbon nanotubes onto carbon fibers by poly(amidoamine) for enhancing interfacial strength in carbon fiber composites. J Mater Chem. 2012;22(13):5928–31.

27. Qian H, Bismarck A, Greenhalgh ES, Kalinka G, Shaffer MSP. Hierarchical composites reinforced with carbon nanotube grafted fibers: the potential assessed at the single fiber level. Chem Mater. 2008;20(5):1862–9.

28. Lee G, Sung M, Youk JH, Lee J, Yu W-R. Improved tensile strength of carbon nanotube-grafted carbon fiber reinforced composites. Compos Struct. 2019;220:580–91.

29. Wang C, et al. The role of grafting force and surface wettability in interfacial enhancement of carbon nanotube/carbon fiber hierarchical composites. Carbon. 2014;69:239–46.

30. Li Y, et al. Tuning the interfacial property of hierarchical composites by changing the grafting density of carbon nanotube using 1,3-propodiamine. Compos Sci Technol. 2013;85: 36–42,.

31. Mei H, et al. Interfacial modification and enhancement of toughening mechanisms in epoxy composites with CNTs grafted on carbon fibers. Compos Sci Technol. 2016;134:89–95.

32. Qin J, et al. Uniform growth of carbon nanotubes on carbon fiber cloth after surface oxidation treatment to enhance interfacial strength of composites. Compos Sci Technol. 2020;195:108198.

33. Khan S, Singh Bedi H, Agnihotri PK. Augmenting mode-II fracture toughness of carbon fiber/epoxy composites through carbon nanotube grafting. Eng Fract Mech. 2018;204:211–20.

34. Kim KJ, Yu W-R, Youk JH, Lee J. Degradation and healing mechanisms of carbon fibers during the catalytic growth of carbon nanotubes on their surfaces. ACS Appl Mater Interface. 2012;4(4):2250–8.

35. Zhang Q, Liu J, Sager R, Dai L, Baur J. Hierarchical composites of carbon nanotubes on carbon fiber: Influence of growth condition on fiber tensile properties. Compos Sci Technol. 2009;69(5):594–601.

36. Qian H, Bismarck A, Greenhalgh ES, Shaffer MSP. Carbon nanotube grafted carbon fibres: a study of wetting and fibre fragmentation. Compos Part A Appl Sci Manuf. 2010; 41(9):1107–14.

37. Lv P, et al. Increasing the interfacial strength in carbon fiber/epoxy composites by controlling the orientation and length of carbon nanotubes grown on the fibers. Carbon. 2011;49(14):4665–73.

38. Liu ZF, et al. Hierarchically buckled sheath-core fibers for superelastic electronics, sensors, and muscles. Science. 2015; 349(6246):400–4.

39. Mu J, et al. Sheath-run artificial muscles. Science. 2019; 365(6449):150–5.

40. Lu H, Baughman RH, Haque MH, Fang SD. Method of fabricating carbon nanotube sheet scrolled fiber reinforced polymer composites and compositions and uses thereof. US9758628B2, 2017 Sep 12.

41. Sohail T, et al. Simulation of surface asperities on a carbon fiber using molecular dynamics and fourier series decomposition to predict interfacial shear strength in polymer matrix composites. Compos Interface. 2022;29(8):947–70.

42. Saito H, et al. Effect of ply-thickness on impact damage morphology in CFRP laminates. J Reinf Plastics Compos. 2011;30(13):1097–106.

43. Li J, et al. Correlations between percolation threshold, dispersion state, and aspect ratio of carbon nanotubes. Adv Funct Mater. 2007;17(16):3207–15.

44. Spitalsky Z, Tasis D, Papagelis K, Galiotis C. Carbon nanotube–polymer composites: chemistry, processing, mechanical and electrical properties. Prog Polym Sci. 2010; 35(3):357–401.

45. Zhao ZJ, et al. MWCNT modified structure-conductive composite and its electromagnetic shielding behavior. Compos Part B Eng. 2017;130:21–7.

46. El-Dessouky HM. 6 Spread tow technology for ultra lightweight CFRP composites: potential and possibilities.

Advanced composite materials: properties and applications. Warsaw: De Gruyter Open Poland; 2017. p. 323–48.

47. Ohlsson F. An introduction to spread tow reinforcements. Part 2: design and applications. Reinf Plastics. 2015;59(5): 228–32.

48. Kim SH, et al. Harvesting electrical energy from carbon nanotube yarn twist. Science. 2017;357(6353):773–8.

49. American Society for Testing and Materials. Standard test method for compressive properties of polymer matrix composite materials using a combined loading compression (CLC) test fixture. ASTM International; 2016.

50. American Society for Testing and Materials. Standard test method for short-beam strength of polymer matrix composite materials and their laminates. ASTM International; 2016.

51. American Society for Testing and Materials. Standard test method for determination of the mode II interlaminar fracture toughness of unidirectional fiber-reinforced polymer matrix composites. ASTM International; 2016.

52. Naik NK, Tiwari SI, Kumar RS. An analytical model for compressive strength of plain weave fabric composites. Compos Sci Technol. 2003;63(5):609–25.

53. Cao Y, et al. Predicting the tensile and compressive failure behavior of angle-ply spread tow woven composites. Compos Struct. 2020;234:111701.

54. Bhushan B, Ling X, Jungen A, Hierold C. Adhesion and friction of a multiwalled carbon nanotube sliding against single-walled carbon nanotube. Phys Rev B. 2008;77(16):1 65428.

55. Kis A, Jensen K, Aloni S, Mickelson W, Zettl A. Interlayer forces and ultralow sliding friction in multiwalled carbon nanotubes. Phys Rev Lett. 2006;97(2):025501.

56. Viet NV, Kuo WS. Load transfer in fractured carbon nanotubes under tension. Compos Part B Eng. 2012;43(2): 332–39.

57. Thostenson ET, Chou T-W. Carbon nanotube networks: sensing of distributed strain and damage for life prediction and self healing. Adv Mater. 2006;18(21):2837–41,.

58. Böger L, Wichmann MHG, Meyer LO, Schulte K. Load and health monitoring in glass fibre reinforced composites with an electrically conductive nanocomposite epoxy matrix. Compos Sci Technol. 2008;68(7):1886–94.

59. Kumar SSA, Uddin MN, Rahman MM, Asmatulu R. Introducing graphene thin films into carbon fiber composite structures for lightning strike protection. Polym Compos. 2019;40(S1):E517–25.

60. Lin W, Wang Y, Yousefpour K, Park C, Kumar V. Evaluating the lightning strike damage tolerance for CFRP composite laminates containing conductive nanofillers. Appl Compos Mater. 2022;29(4):1537–54.

61. Arai M, Noro Y, Sugimoto K, Endo M. Mode I and mode II interlaminar fracture toughness of CFRP laminates toughened by carbon nanofiber interlayer. Compos Sci Technol. 2008;68(2):516–25.

62. Czabaj MW, Davidson BD. Determination of the mode I, mode II, and mixed-mode I–II delamination toughness of a graphite/polyimide composite at room and elevated temperatures. J Compos Mater. 2016;50(16):2235–53.

63. Bonhomme J, Argüelles A, Viña J, Viña I. Fractography and failure mechanisms in static mode I and mode II delamination testing of unidirectional carbon reinforced composites. Polym Test. 2009;28(6):612–7.

64. Zhou HX, et al. Mode II interlaminar fracture of hybrid woven carbon-Dyneema composites. Compos Part A Appl Sci Manuf. 2020;131:105785.